Available online at www.sciencedirect.com

SCIENCE DIRECT

Lithos 77 (2004) 493–510

LITHOS

www.elsevier.com/locate/lithos

Petrological constraints on seismic properties of the Slave upper mantle (Northern Canada)☆

M.G. Kopylova[a,*], J. Lo[a], N.I. Christensen[b]

[a] Geological Sciences Division, Earth and Ocean Sciences, The University of British Columbia, 6339 Stores Road, Vancouver, British Columbia, Canada, V6T 1R9

[b] Department of Geology and Geophysics, University of Wisconsin-Madison, Madison, WI, USA

Received 27 June 2003; accepted 21 January 2004
Available online 28 May 2004

Abstract

Modes and compositions of minerals in Slave mantle xenoliths, together with their pressures and temperatures of equilibrium were used to derive model depth profiles of P- and S-wave velocities (Vp, Vs) for composites equivalent to peridotite, pyroxenite and eclogite. The rocks were modeled as isotropic aggregates with uniform distribution of crystal orientations, based on single-crystal elastic moduli and volume fractions of constituent minerals. Calculated seismic wave velocities are adjusted for in situ pressure and temperature conditions using (1) experimental P- and T- derivatives for bulk rocks' Vp and Vs, and (2) calculated P- and T- derivatives for bulk rocks' elastic moduli and densities. The peridotite seismic profiles match well with the globally averaged *IASP91* model and with seismic tomography results for the Slave mantle. In peridotite, an observed increase of seismic wave velocities with depth is controlled by lower degrees of chemical depletion in the deeper upper mantle. In eclogite, seismic velocities increase more rapidly with depth than in peridotite. This follows from contrasting first-order pressure derivatives of bulk isotropic moduli for eclogite and peridotite, and from the lower compressibility of eclogite at high pressures. Our calculations suggest that depletion in cratonic mantle has a distinct seismic signature compared to non-cratonic mantle. Depleted mantle on cratons should have slower Vp, faster Vs and should show lower Poisson's ratios due to an orthopyroxene enrichment. For the modelled Slave craton xenoliths, the predicted effect on seismic wave velocities would be up to 0.05 km/s.

Keywords: Seismic velocity; Slave mantle; Eclogite; Peridotite; Chemical depletion; Density

1. Introduction

More than 20 years ago, the pioneering work of Jordan (1979) established links between density, elastic properties and the bulk composition of peridotitic mantle. Since then we have begun to understand better the compositional contrast between Archean cratonic mantle and younger non-cratonic mantle (Boyd, 1999; Kelemen et al., 1998). This paper aims at analysing compositional effects on seismic properties of cratonic mantle.

The analysis is carried out for mantle rocks of the Slave craton found as kimberlite-derived xenoliths.

☆ Supplementary data associated with this article can be found, in the online version, at doi: 10.1016/j.lithos.2004.03.012.

* Corresponding author. Tel.: +1-604-822-0865.
E-mail address: mkopylov@eos.ubc.ca (M.G. Kopylova).

0024-4937/$ - see front matter © 2004 Elsevier B.V. All rights reserved.
doi:10.1016/j.lithos.2004.03.012

These mantle rocks are characterized mineralogically and geochemically, and comprehensive data on their modal mineralogy, mineral chemistry and pressures and temperatures of equilibria are available. For this study, these bulk characteristics are combined with the latest experimental data on elastic properties of end-member components of mineral solid solutions (i.e. reviews by Vacher et al., 1998; Hofmeister and Mao, 2003; Ji et al., 2003). Sufficient experimental data now exist for estimating the bulk elastic properties of a mantle rock with good accuracy if the mineralogy of the rock is known (Gregoire et al., 2001; Hofmeister and Mao, 2003).

The Slave mantle is an excellent natural laboratory for analysing compositional effects on seismic properties of cratonic mantle as it provides samples of variously depleted peridotite, pyroxenite and compositionally diverse eclogite. The modelling used in this study determines the contrast in seismic properties in different mantle lithologies and the range of seismic velocities expected for a naturally heterogeneous mantle section. We find that eclogite stands out when compared with other mantle rocks because of its faster increase of compressional and sheared wave velocities (Vp and Vs) with depth. Our calculations also suggest a distinct seismic signature indicating depletion in the cratonic mantle.

2. Samples and analytical techniques

This study is based on mantle xenoliths derived from the Jericho and 5034 kimberlites on the Slave craton (northern Canada). The Slave craton, stabilized at 2.6 Ga, represents a small Archean nucleus to the larger Proterozoic North American craton. The kimberlites are located in the northern and southeastern parts of the Slave Craton (Fig. 1). The Jericho pipe is dated as Middle Jurassic (172 ± 2 Ma by Rb-Sr and U-Pb geochronology) and the 5034 kimberlite of the Gahcho Kue cluster as Middle Cambrian (539 ± 2 Ma by the Rb-Sr method on phlogopite) (Heaman et al., 2003). We studied all mantle lithologies typical of the cratonic mantle, i.e., peridotite, pyroxenite and eclogite. The mantle peridotites and pyroxenite that are the basis for this study were previously described in several papers (Table 1) which reported the petrology and bulk and mineral compositions.

Eclogitic xenoliths make up ∼ 25% of all mantle xenoliths in the Jericho kimberlite, and ∼ 18% in the 5034 kimberlite. This work presents new data on mineral compositions, pressures and temperatures of equilibrium, and modal mineralogy for 13 new samples of the Jericho eclogite whose elastic properties are modelled (Supplementary Electronic Tables 1 and 2).

Mineral modes were estimated using image analysis techniques applied to scanned images of 2 cm × 4 cm thin sections of eclogite. Digital images were acquired using a Polaroid Sprintscan® 35 on thin sections that were cut thicker than normal (>30 microns) to lend stronger body colour to garnet. The images were captured with a polarized light source, enhanced, and analysed using free image analysis software NIH Image 1.62 (http://rsb.info.nih.gov/nih-image/). It was possible to determine modal abundances of secondary clinopyroxene and garnet because of their distinctly finer grain size which give them darker colours. The precision on the modal estimates by the image analysis method is estimated to be 2.5% (Kopylova and Russell, 2000).

Minerals in the eclogites were analysed using an automated CAMECA SX-50 microprobe (Department of Earth and Ocean Sciences, University of British Columbia, Canada) at an accelerating voltage of 15 kV and with a 20-mA beam current. On-peak counting times were 10 s for major elements, and 60 s for K in clinopyroxene and Na in garnet. Primary phases in a sample were analysed as 8–15 points in cores and rims of 4–5 grains. Analyses with poor stoichiometry and totals were excluded and mineral compositions were averaged over 3–12 analyses for homogeneous phases or presented as individual analyses for inhomogeneous minerals (Supplementary Electronic Table 2).

In eclogite of the 5034 kimberlite, all primary minerals, with the exceptions of garnet (20–30%) and rutile (2%), are completely altered to serpentine, chlorite and phlogopite. Limited observations on mineralogical and textural characteristics of these rocks suggest that the 5034 eclogite resemble that of Jericho. Severe weathering of the 5034 eclogite prevents detailed petrographic and petrophysical work, and only Jericho eclogite was used as the basis for this study.

Eclogite xenoliths from Jericho are fresh and are composed of primary pyrope, omphacite and rutile, with occasional zircon, olivine, orthopyroxene, kya-

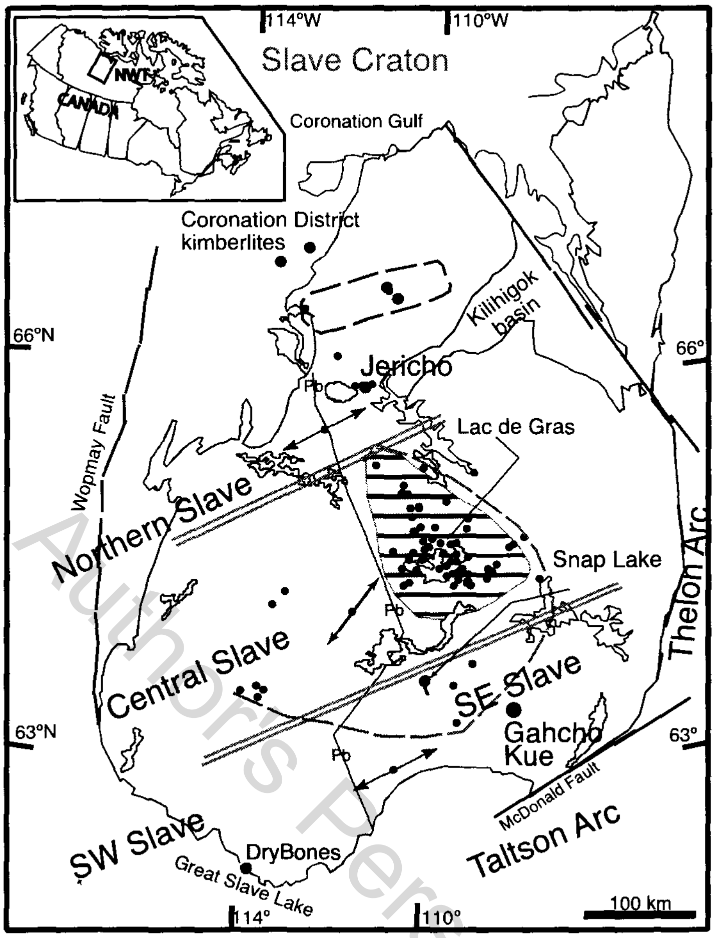

Fig. 1. Schematic map of the Slave craton (Northwest Territories, Canada—see inset), showing the location of kimberlite pipes (black dots). Double lines designate the boundaries between northern, central and southern lithospheric domains as distinguished by distinct compositions of garnet in kimberlite concentrates (Grütter et al., 1999). The SW and SE Slave terranes may be separated by the Pb isotopic boundary of Thorpe et al. (1992) (thin solid line). The darker area is the postulated surface and subsurface extent of the Central Slave Basement Complex (protocraton of Ketchum and Bleeker, 2001). Orientation of the S-wave polarization (bars with arrows) indicates the directions of anisotropy of the mantle (Bank et al., 2000). Also shown are the minimum extents of a shallow ultra-depleted layer (horizontal lined pattern) and of the deeper Archean lherzolitic layer (Griffin et al., 1999b) of the Central Slave (dashed outlines).

nite, apatite and ilmenite. Omphacitic clinopyroxene commonly comprises 60–75% of the eclogite (Supplementary Electronic Table 2). Detailed mineralogical work on these specimens revealed the presence of two late mineral assemblages. The first, which we consider mantle metasomatic and pre-kimberlitic, relates to partial recrystallization of garnet and clinopyroxene and their replacement by phlogopite and amphibole. Spongy rims of recrystallized, secondary clinopyroxene enriched in Ti, Ca and Mg, and depleted in the jadeitic component (Supplementary Electronic Table 1), may overgrow primary omphacite and replace up to half of it. Pyrope may also be overgrown by rims of late, Mg $\pm$ Ti-rich and Ca-poor garnet or, more commonly, by amphibole. The second mineral assemblage comprises epidote, chlorite and serpentine that mark shallow retrograde alteration of the eclogite. The Jericho eclogite is subdivided into two groups based on the presence of massive or foliated fabric; the foliated texture is partly controlled by preferential replacement of garnet and clinopyroxene by secondary volatile-rich phases along specific planes. The

Table 1
Types and characteristics of Slave mantle xenoliths

Location	Rock type	Depth, km[a]	Comments	Reference
Jericho (N Slave)	Low-*T* spinel peridotite	35–100	Chemically depleted	mineral analyses are from McCammon and Kopylova (accepted pending revisions); modes and bulk compositions are from Kopylova and Russell (2000)
Jericho (N Slave)	Low-*T* spinel-garnet peridotite	80–170		Petrology and mineral analyses are from Kopylova et al. (1999a); modes and bulk compositions are from Kopylova and Russell (2000)
Jericho (N Slave)	Low-*T* garnet peridotite	120–185		
Jericho (N Slave)	High-*T* garnet peridotite	165–194	Deformed, not equilibrated on a steady-state geotherm	
Jericho (N Slave)	Low-*T* and high-*T* fertile garnet peridotite		Enriched in modal clinopyroxene and garnet	
Jericho (N Slave)	Pyroxenite	200–215	Megacrystalline	
5034 (SE Slave)	Low-*T* spinel peridotite	35–100	Chemically depleted	Kopylova and Caro (2004)
5034 (SE Slave)	Low-*T* garnet peridotite	215–260	Coarse or deformed	

[a] Estimated according to the Brey and Köhler (1990) thermobarometry.

massive and foliated eclogites differ in mineral composition (Kopylova et al., 1999b), bulk composition and origin (Kopylova, 2003). The protolith for the foliated eclogite may have been low-pressure mafic rocks that formed partly as plagioclase cumulates. The protoliths for the massive eclogite may have been deeper high-P cumulates of mafic magmas.

3. Experimental methods

Laboratory determination of acoustic velocity and density was performed at the Rock Physics Lab at Purdue University on mini-cores of approximately 2 cm in diameter and more than 3 cm in length. Where possible, three cores were cut for a sample; A-core was perpendicular to foliation, B-core was parallel to lineation in the foliation plane, and C-core was perpendicular to lineation in the foliation plane. For smaller samples only A- and B-cores were cut. Compressional and shear wave velocities polarized at A and B directions were measured on each core samples at hydrostatic confining pressures up to 1000 MPa using the pulse transmission technique (Christensen, 1965) and 1-MHz transducers. The error in the laboratory velocity measurements was evaluated to be less than 0.5% for Vp and 1% for Vs (Christensen and Shaw, 1970). The bulk density of each core was calculated from its mass and dimensions.

4. Measured elastic properties

Acoustic velocities and density were measured in four eclogite xenoliths chosen to represent the foliated and massive types. Measured Vp and Vs at different confining pressures (Supplementary Electronic Table 3) are plotted on Fig. 2. An extrapolation of the linear fits of velocity–pressure curves at P>600 MPa, where microcracks are closed, yields Vp and Vs at room temperature and pressure (Fig. 2). Vp in Jericho eclogite varies from 6.25 to 7.9 km/s, and Vs from 3.5 to 4.4 km/s. The velocities are strongly controlled by modal mineralogy. In fresh eclogite rocks 26-6 and F6NEcl Vp = 7.25–7.9 and Vs = 3.9–4.4 km/s, whereas in retrograde eclogite, where primary omphacite is almost totally replaced by chlorite + epidote ± phlogopite and amphibole, the velocities are much lower. Massive eclogite 26-6

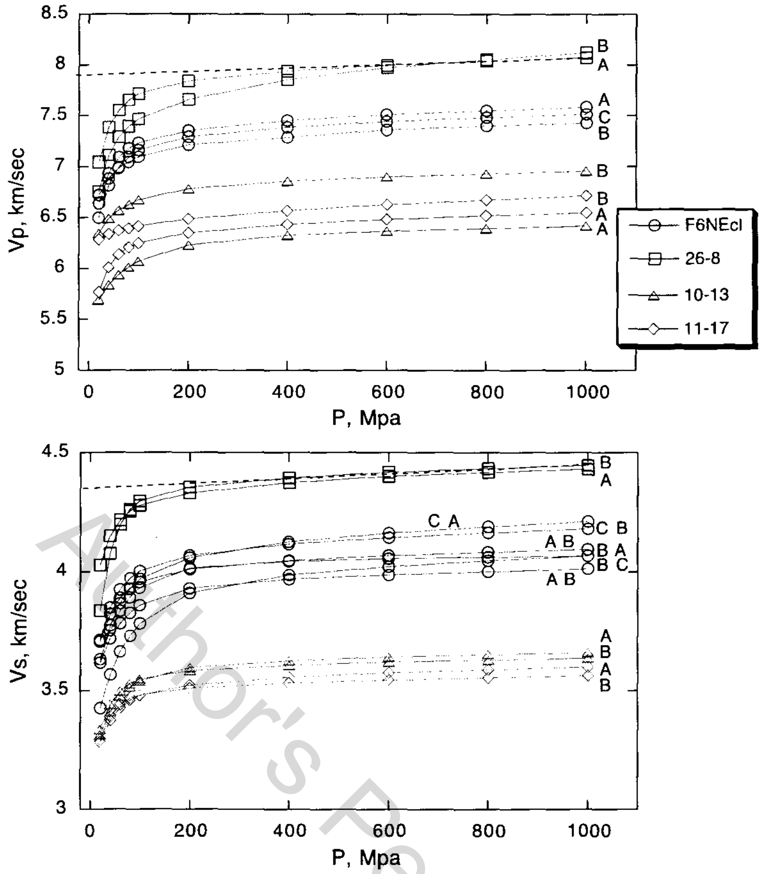

Fig. 2. Laboratory-measured velocity–pressure curves for the Jericho eclogite. Letter after sample number indicates direction of the wave propagation. For Vs measurements, the first letter designates the propagation direction, second letter—the vibration direction. Dashed lines extrapolate seismic velocities for atmospheric pressures.

shows Vp and Vs values that exceed those for all samples of foliated eclogite.

Vp anisotropy varies in Jericho eclogite from 0% to 8.1%. Massive fresh eclogite 26-6 shows no anisotropy, fresh anisotropic sample F6NEcl has 2% Vp anisotropy, and a maximum anisotropy of 8% is recorded in sample 10–13, where it is density-related. Large variations in density from 2.971 in the A direction to 3.108 in the B direction reflect uneven development of the secondary chlorite–epidote–phlogopite aggregate (65% of the rock).

Vs anisotropy (1.3–3.4%) is detected only in sample F6NEcl. In all other samples it does not exceed 1%. Shear wave splitting was measured only in sample F6Necl. It is relatively large (2%) only in the A direction and is practically nonexistent in the B and C directions. It reflects strong polarizing properties of the foliation plane where waves parallel and normal to the lineation propagate with different velocities.

5. Calculated elastic properties

5.1. Elastic properties at the surface

Seismic velocities (Vp, Vs) of the mantle rocks were estimated from high-precision single crystal elastic moduli and volume fractions of constituent minerals using appropriate mixture rules. They describe variations of effective elastic moduli of polymineralic composites as a function of their end-member elastic moduli and volume fractions. It has been shown that the mean Vp of a polymineralic rock is exclusively controlled by the volume fractions of its constituent minerals, while grain shape, crystallographic preferred orientations, anisotropy and other perturbations have minimal effects (Ji et al., 2003). Therefore, we computed average velocities for mantle rocks as for isotropic aggregates with uniform distribution of crystal orientations. Several mixture rules were proposed for such calculations: the Reuss average, the Voigt average, their arithmetic (known as the Hill) average or geometrical mean (reviewed in Ji et al., 2003), and the average of the Hashin–Shtrikman bounds (Bina and Helffrich, 1992). Since the Hill average remains the most widely used mixture rule for predictions of seismic velocities in isotropic polycrystalline mixtures (e.g. Long and Christensen, 2000; Gregoire et al., 2001), and gives results similar to the more complex iterative Hashin–Shtrikman method (Bina and Helffrich, 1992), it was employed for the computations.

These methods require knowledge of the volume percentage of mineral end-members in a rock. Here, volume percentages were calculated based on mineral modes and volume fractions of end-member components which, in turn, were estimated based on compositions of mineral solid solutions. We expressed the mineral solid solutions as ideal mixtures of appropriate components with known elastic properties. Olivine, orthopyroxene and spinel were recalculated as mixtures of Fe and Mg end-members, whereas clinopyroxene and garnet were modelled more elaborately (Table 2). Cr_2O_3 in garnet, which may range up to 20 wt.% in cratonic peridotite, was accounted for using an uvarovite end-member. Although the andradite component in mantle garnets is not very significant, we assigned all Fe^{3+} estimated stoichiometrically to andradite. Clinopyroxene in studied rocks contains significant amounts of Na, Al and Cr. Since elastic moduli data are not available for Cr end-members of clinopyroxene, and the elastic

Table 2
Densities and elastic moduli for minerals and mineral end-members

Component	Composition	Adiabatic bulk modulus K_S, GPa	Shear modulus G, GPa	Density, g/cm^3 [a]	Source
Forsterite	Mg_2SiO_4	128	81	3.222	Duffy and Ahrens (1995), Li et al. (1996), Zha et al. (1996, 1997)
Fayalite	Fe_2SiO_4	128	50	4.404	Duffy and Ahrens (1995), Li et al. (1996), Zha et al. (1996, 1997)
Enstatite	$Mg_2Si_2O_6$	104	74.9	3.215	Flesch et al. (1998), Vacher et al. (1998)
Ferrosilite	$Fe_2Si_2O_6$	124	54	4.014	Angel and Hugh-Jones (1994), Chai et al. (1997)
Jadeite	$NaAlSi_2O_6$	126	84	3.320	Zhao et al. (1997), Kandelin and Weidner (1998)
Diopside	$CaMgSi_2O_6$	105	67	3.277	Zhang et al. (1997), Sumino and Anderson (1984)
Hedenbergite	$CaFeSi_2O_6$	118	61	3.657	Zhang et al. (1997), Sumino and Anderson (1984)
Pyrope	$Mg_3Al_2(SiO_4)_3$	173	92	3.600	Vacher et al. (1998)
Almandine	$Fe_3Al_2(SiO_4)_3$	180	99	4.328	Chen et al. (1996)
Grossular	$Ca_3Al_2(SiO_4)_3$	168	107	3.597	Isaak et al. (1992)
Andradite	$Ca_3Fe_2(SiO_4)_3$	157	90	3.836	Bass, 1986
Uvarovite	$Ca_3Cr_2(SiO_4)_3$	162	92	3.85	Bass, 1986
Spinel	$MgAl_2O_4$	197.9	108.5	3.582	Yoneda (1990), Chang and Barsch (1973)
Hercinite	$FeAl_2O_4$	210.3	84	4.258	Wang and Simmons, 1972
Phlogopite [b]		50	25.2	2.820	Yang and Prewitt, 2000
Hornblende		87.1	43.2	3.120	Hearmon, 1984
Ilmenite		212.3	132.3	3.795	Weidner and Ito, 1985
Apatite		84.3	60.7	3.200	Hearmon, 1984
Rutile		211.5	113.1	4.240	Isaak et al., 1998
Chlorite		81.0	43.1 [c]	2.800	Collins and Catlow (1992); Welch and Crichton (2002)

[a] Densities are after Duffy and Anderson (1989) except when indicated.
[b] Density is from Christensen (1989), and G is calculated from Vs of Christensen (1989).
[c] Data for mica.

moduli of Ca-tchermakite (Ca-Ts) were shown to be reasonably well approximated by those of jadeite (Gregoire et al., 2001), the "jadeite" abundances in Table 3 refer to combined volume percentages of cosmochlore ($NaCrSi_2O_6$), Ca-tchermakite ($CaAlAlSiO_6$), and jadeite ($NaAlSi_2O_6$). Fortunately, in eclogites, where modes of clinopyroxene are high, molar fractions of Ca-Ts and cosmochlore in omphacites are negligible, and the absence of experimentally determined elastic parameters for them does not affect the calculations. We used the most recent experimentally determined densities and elastic properties available for the mineral end-members (Table 2).

The resulting volume proportions of fixed composition minerals and end-member components for individual xenoliths of peridotite and pyroxenite are given in Supplementary Electronic Table 4. Various types of peridotites were also characterized by mean mineral modes (Kopylova and Russell, 2000; Kopylova and Caro, 2004). Calculated abundances of end-member components for them and for individual eclogite xenoliths are listed in Table 3.

Seismic velocities modelled at the surface can be checked against those measured experimentally. An excellent match between the two is observed in sample 26-6 (7.92 vs. 7.82 km/s and 4.56 vs. 4.36 km/s; Table 3). In all other samples, measured velocities are lower than those calculated, even when secondary chlorite is compensated for. The difference is 0.2 km/s in a sample with 25% chlorite pseudomorphs, and 1.1 km/s in severely altered samples 11–17 and 10–13 with 65% chlorite. A factor that contributes to this discrepancy may be a higher porosity of altered retrograde eclogite, which makes the pores remain open at higher pressures and leads to underestimation of measured ultrasonic velocities in xenoliths (Soedjatmiko and Christensen, 2000).

5.2. Elastic properties at depth

Knowledge of accurate ambient pressures and temperatures for mantle lithologies is central to modelling mantle seismic profiles because seismic properties are strongly dependent on $P-T$ variations. Pressures and temperatures were estimated by two methods, both of which satisfy available petrological constraints for the Jericho and 5034 xenolith suites, i.e. (1) the two-pyroxene geothermometer of Brey and Köhler (1990) (BKN) and the Al-in-Opx geobarometer of Brey and Köhler (1990) (BK); and (2) the geothermometer of Finnerty and Boyd (1987) (FB) and the geobarometer of MacGregor (1974) (MC) (Table 3). Pseudo-univariant pressure–temperature lines for eclogite samples have been calculated by garnet-clinopyroxene geothermometry using both the Ellis and Green (1970) (EG) and the Ai (1994) formulations with all Fe calculated as Fe^{2+}. The rationale for this choice was discussed in detail in Kopylova et al. (1999b). The Ai thermometry was used only in conjunction with the FB-MC peridotitic geotherm, whereas the EG thermometry was used only in conjunction with the BKN-BK peridotitic geotherm (Table 3). These combinations of eclogitic and peridotitic thermobarometry were chosen to satisfy a petrological constraint based on the diamondiferous character of some of the Jericho eclogites (Kopylova et al., 1999b).

Two methods were used to estimate seismic wave velocity at depth. First, calculated seismic wave velocities at the surface were adjusted for pressures and temperatures corresponding to mineral equilibration at depth. Temperature and pressure derivatives employed in these computations are listed in Table 4. Pressure derivatives for eclogite were calculated from high-pressure measurements on samples JDF6Necl and 26-6, which are the least altered samples and are practically chlorite-free. The temperature derivatives for eclogites and all derivatives for peridotite and pyroxenite were calculated based on high-frequency ultrasonic studies reported elsewhere (Table 4). We considered only measurements for unaltered samples that were close in mineralogy to the samples studied here. Table 4 also shows that the generalized values of seismic wave velocity derivatives for all mantle and lower crust lithologies, and for pyrolite, are similar to those used in this study. The pyrolite derivatives were estimated based on the Mie–Gruneisen's equation of state and single crystal elastic data at temperatures of 500, 1000 and 1500 °C (Bina and Helffrich, 1992).

The second method directly computes Vp and Vs of mineral end-members at high P and T by accounting for the pressure and temperature dependence of their elastic moduli and densities. We used the method of Fei (1995) for a subset of representative samples of eclogite and peridotite. The solution requires tabulated

Table 3
Calculated abundances (vol.%) of end-member components and seismic speeds at surface and at depth for averaged types of peridotite and for individual samples of eclogite

Rock type	Jericho peridotites and pyroxenite						5034 peridotites	
	Spl peridotite	Spl-Gar peridotite	Low-T Gar peridotite	Fertile Gar peridotite	High-T Gar peridotite	Pyroxenite	Spl peridotite	Low-T Gar peridotite
Average of	12	7	6	5	9	2	5	24
Forsterite	67.7	66.6	67.9	56.5	71.5	20.4	74.9	72.1
Fayalite	4.0	4.2	4.9	3.4	5.5	1.8	4.1	4.6
Enstatite	24.3	20.2	16.3	15.8	14.3	26.4	18.0	14.0
Ferrosilite	1.5	1.2	1.1	0.9	1.0	2.4	1.2	0.8
Jadeite	0.1	0.3	0.6	1.6	0.3	3.4	0.0	0.3
Diopside	1.3	2.9	3.9	8.7	2.1	25.1	0.6	2.2
Heldenbergite	0.1	0.2	0.3	0.6	0.2	2.8	0.0	0.2
Almandine	0.0	0.6	0.8	1.6	0.7	3.1	0.0	0.8
Pyrope	0.0	2.7	3.7	9.2	3.7	12.5	0.0	4.0
Grossular	0.0	0.1	0.0	0.0	0.0	0.4	0.0	0.0
Andradite	0.0	0.0	0.0	0.0	0.0	0.0	0.0	0.1
Uvarovote	0.0	0.5	0.6	1.7	0.7	1.7	0.0	1.0
$MgAl_2O_4$	0.6	0.2	0.0	0.0	0.0	0.0	0.8	0.0
$FeAl_2O_4$	0.4	0.4	0.0	0.0	0.0	0.0	0.4	0.0
Total	100.0	100.0	100.0	100.0	100.0	100.0	100.0	100.0
Rock Mg-number	92.9	92.0	91.8	89.0	90.6		92.6	91.2
Density	3.287	3.308	3.318	3.340	3.319	3.380	3.286	3.314
Vp Hill, km/s	8.27	8.29	8.29	8.31	8.31	8.11	8.32	8.34
Vs Hill, km/s	4.85	4.85	4.84	4.84	4.84	4.73	4.87	4.86
Lower P–T limit								
T FB, deg C	450	650	760	1020	1120	1115	450	970
P MC, GPa	1.09	2.42	3.40	5.17	5.77	5.65	1.10	5.20
Vp at depth, km/s	8.14	8.18	8.18	8.27	8.28	7.68	8.19	8.33
Vs at depth, km/s	4.77	4.78	4.80	4.83	4.83	4.73	4.79	4.86
T BKN, deg C	450	640	840	1070	1280	1200	610	1130
P BK, GPa	1.1	2.5	3.6	4.9	5.0	6.0	1.1	6.5
Vp at depth, km/s	8.14	8.19	8.19	8.21	8.10	7.63	8.09	8.37
Vs at depth, km/s	4.77	4.79	4.78	4.79	4.72	4.73	4.74	4.89
Higher P–T limit								
T FB, deg C	780	860	1090	1190	1250	1135	680	1190
P MC, GPa	3.30	4.00	5.70	5.85	6.35	5.71	3.00	5.80
Vp at depth, km/s	8.18	8.22	8.18	8.24	8.26	7.66	8.25	8.26
Vs at depth, km/s	4.80	4.81	4.83	4.81	4.82	4.73	4.83	4.83
T BKN, deg C	750	1000	1100	1120	1310	1250	830	1290

P BK, GPa	3.00	4.90	5.50	5.80	5.80	6.50	3.00	7.90
Vp at depth, km/s	8.16	8.23	8.24	8.28	8.17	7.63	8.16	8.43
Vs at depth, km/s	4.79	4.82	4.81	4.83	4.77	4.74	4.78	4.93

Sample	Jericho eclogite																	
	Primary paragenesis													Mantle metasomatic paragenesis				
	6-11	20-7	16-4	55-4	JDF6N-Ec13	52-5	47-2	42-3	47-8	26-6	11-17	10-13	JDF6NEcl	55-4	52-5	47-2	42-3	47-8
"Jadeite"	9.4	13.5	8.2	18.1	17.9	22.1	20.1	17.9	26.3	7.4	36.4	38.6	28.2	16.2	21.7	18.9	14.1	13.9
Diopside	52.9	30.6	52.8	24.7	35.3	37.0	40.5	33.4	24.0	53.2	22.8	25.2	33.2	26.1	36.3	40.5	38.7	36.0
Hedenbergite	12.9	5.8	7.3	4.7	8.0	5.0	8.5	9.8	10.2	6.3	8.9	9.8	7.1	5.0	4.9	8.6	8.4	12.0
Almandine	7.3	15.4	8.0	15.3	15.1	8.0	11.8	14.0	15.6	5.1	12.2	10.4	9.9	17.3	7.8	12.7	13.9	13.3
Pyrope	6.9	18.0	19.0	21.8	16.2	19.7	12.0	11.2	8.4	19.8	6.7	5.7	9.2	20.6	18.4	10.8	9.2	5.9
Grossular	2.2	8.7	3.8	15.1	6.5	4.7	6.6	5.4	8.3	2.6	9.5	7.9	7.9	14.2	4.1	5.9	4.5	5.9
Andradite	0.3	0.0	0.6	0.0	0.4	0.3	0.3	0.3	0.7	0.3	0.0	0.0	0.0	0.0	0.3	0.3	0.3	0.5
Uvarovite	0.0	0.0	0.0	0.0	0.0	0.0	0.0	0.0	0.0	0.3	0.0	0.0	0.0					
Orthopyroxene	0.3	0.0	0.0	0.0	0.0	0.0	0.0	0.0	0.0	0.0	0.0	0.0	0.0					
Apatite	0.0	0.0	0.0	0.0	0.0	0.0	0.0	0.0	0.0	0.0	0.5	0.0	0.0					
Rutile	2.1	0.0	0.0	0.3	0.2	0.0	0.2	5.1	0.5	0.0	3.0	2.5	0.0	0.3	0.0	0.2	5.1	0.5
Ilmenite	0.0	0.0	0.4	0.0	0.0	0.0	0.0	0.0	0.0	0.4	0.0	0.0	0.0	0.3	3.2	1.1	2.9	5.9
Phlogopite	5.7	8.0	0.0	0.0	0.4	3.0	0.0	2.9	6.0	4.7	0.0	0.0	4.5	0.0	3.1	1.0	2.9	5.9
Chlorite																		
Total	100.0	100.0	100.0	100.0	100.0	100.0	100.0	100.0	100.0	100.0	100.0	100.0	100.0	100.0	100.0	100.0	100.0	100.0
Density, g/cm^3	3.431	3.516	3.471	3.585	3.549	3.453	3.505	3.560	3.526	3.413	3.536	3.508	3.455	3.599	3.439	3.503	3.538	3.476
Vp Hill, km/s	7.75	7.97	8.10	8.44	8.20	8.13	8.16	8.09	8.00	7.92	8.29	8.25	8.03	8.40	8.09	8.09	7.98	7.82
Vs Hill, km/s	4.46	4.57	4.68	4.87	4.73	4.69	4.72	4.65	4.61	4.56	4.82	4.80	4.65	4.84	4.69	4.68	4.58	4.52
Vp measured, km/s										7.82								
Vs measured, km/s										4.36								
T Ai-FB, deg C	713	902	841	1200	861	1013	840	861	1012	n/d[a]	1140	1125	983					
P Ai-FB, GPa	2.93	4.38	4.00	6.20	4.05	5.21	3.90	4.04	5.17	n/d	5.95	5.90	5.00					
Vp at depth, km/s	8.03	8.45	8.53	9.14	8.63	8.71	8.57	8.52	8.58		8.97	8.92	8.59					
Vs at depth, km/s	4.53	4.70	4.80	5.07	4.85	4.87	4.83	4.77	4.78		5.02	5.00	4.82					
T EG-BK, deg C	803	911	928	1290	886	1003	871	867	921	n/d	1012	1002	946					
P EG-BK, GPa	3.70	4.13	4.27	5.50	3.97	4.80	3.86	3.82	4.20	n/d	4.86	4.77	4.38					
Vp at depth, km/s	8.07	8.40	8.55	8.98	8.61	8.64	8.55	8.48	8.44		8.81	8.76	8.49					
Vs at depth, km/s	4.54	4.68	4.80	5.00	4.84	4.84	4.82	4.75	4.72		4.96	4.94	4.78					
Mean Vp anisotropy										0.20%	2.36%	8.10%	2.03%					
Mean Vs anisotropy										0.36%	0.97%	0.36%	1.3–3.38%					
Vs splitting[b]													0.5–2.04%					

[a] Not determined as mineral compositions are outside the range of calibration for the used thermometers.

[b] SKS splitting is calculated as an average for measurements at 600, 800 and 1000 MPa as $200\%*(V_A - V_B)/(V_A + V_B)$.

Table 4
Pressure and temperature derivatives of seismic velocities for mantle rocks

Rock type	Description and source	dVp/dP, km/s × Mpa × 10^{-5}	dVp/dT, km/s × deg × 10^{-5}	dVs/dP, km/s × MPa × 10^{-5}	dVs/dT, km/s × deg × 10^{-5}
Peridotite	Harzburgite with < 16% serpentine (Long and Christensen, 2000)	10.7		6.4	
	Peridotite (Christensen, 1989)		− 60		− 35
	Computation for pyrolite with 15% garnet		− 44 at 500–1000 °C		− 34
	(Bina and Helffrich, 1992)		− 56 at 1000–1500 °C		
Pyroxenite	Pyroxenite (Christensen, 1989)		− 100		− 35
Eclogite	Measurements for 26-6A, F6NEcl	18.1		7.9	
	Chlorite-free eclogite (Kern et al., 1999)		− 36.1		− 24.1
Mantle and lower crust rocks	Jackson et al., 1990; Gregoire et al., 2001	10	− 50		

Temperature derivatives are calculated at P = 300–600 MPa for T = 600–1000 °C (100–300 °C for pyroxenite).
Pressure derivatives are calculated for 25 °C, P = 600–1000 MPa to eliminate the effects of microfracture closing (Long and Christensen, 2000; Kern et al., 1999).

Table 5
P and T derivatives of elastic moduli, thermal expansion coefficients and Andersen–Gruneisen parameters calculated for selected Slave peridotite and eclogite

	Spl peridotite		Eclogite	Source of elastic data for mineral end-members
	11–18	44–12	6–11	
Thermal expansion coefficient, αo (10^{-6})[a]	27.8	27.2	29.4	Fei (1995)
Andersen–Gruneisen parameter, δ_T	4.1	4.2	6.1	Bina and Helffrich (1992), Fei (1995)
First-order P derivative K_S'	4.0	4.3	5.8	Bina and Helffrich (1992), Vacher et al. (1998), Hofmeister and Mao (2003)
First-order P derivative G'	1.1	1.1	1.6	Bina and Helffrich (1992), Vacher et al. (1998), Hofmeister and Mao (2003)
First-order T derivative K_S/dT, GPa/deg	− 0.016	− 0.015	− 0.015	Bina and Helffrich (1992), Vacher et al. (1998)
First-order T derivative G/dT, GPa/deg	− 0.014	− 0.013	− 0.010	Bina and Helffrich (1992), Vacher et al. (1998)
At surface				
Density, g/cm^3	3.284	3.291	3.431	
K_S, GPa	125.6	122.1	110.0	
G, GPa	77.9	77.2	65.2	
Vp, km/s	8.36	8.27	7.58	
Vs, km/s	4.87	4.84	4.36	
At depth				
T, °C	715	647	713	
P, GPa	3.00	2.50	2.93	
Density, g/cm^3	3.296	3.301	3.439	
K_S, GPa	127.0	123.6	116.8	
G, GPa	68.5	69.0	62.9	
Vp, km/s	8.138	8.083	7.637	
Vs, km/s	4.558	4.572	4.275	
Vp calculated using seismic speed derivatives, km/s	8.27	8.16	7.86	
Vs calculated using seismic speed derivatives, km/s	4.82	4.78	4.43	

[a] αo independent of temperature as tabulated in Fei (1995).

data on first-order individual end-member derivatives of isothermal and adiabatic bulk moduli K_T and K_S, shear modulus G, as well as their thermal expansion coefficients and Andersen–Gruneisen parameters (Table 5). These data are now published for almost all end-member components, including non-quadrilateral pyroxenes and garnets, and cover real mineralogies of rocks with sufficient accuracy. Seismic velocities at depth computed in this manner are listed in Table 5.

6. Results

Calculated seismic velocities for the Slave peridotites and eclogite are plotted against depth on Fig. 3. The figure shows individual samples using two sets of pressures and temperatures that are equally good at describing their equilibrium conditions of origin. These two P–T solutions define the similar xenolith-derived geotherm, but may significantly shift depth position of individual samples within the geotherm. The scatter on the resulting plot thus reflects (1) uncertainty in the estimated P–T conditions of rocks, and (2) varying mineral proportions in rocks found at a given depth. The former uncertainty translates to an average velocity variation of 0.02 km/s, although in rare samples the difference can be as high as 0.15 km/s in Vp and 0.1 km/s in Vs. The calculated spread of Vp at a given depth that relates to varying mantle mineralogy reaches 0.3 km/s in peridotite and 0.4 km/s in eclogite. This variation reflecting mantle heterogeneity exceeds errors inherent to methodology of Vp–Vs calculations. An example of the latter is the difference of 0.05 km/s

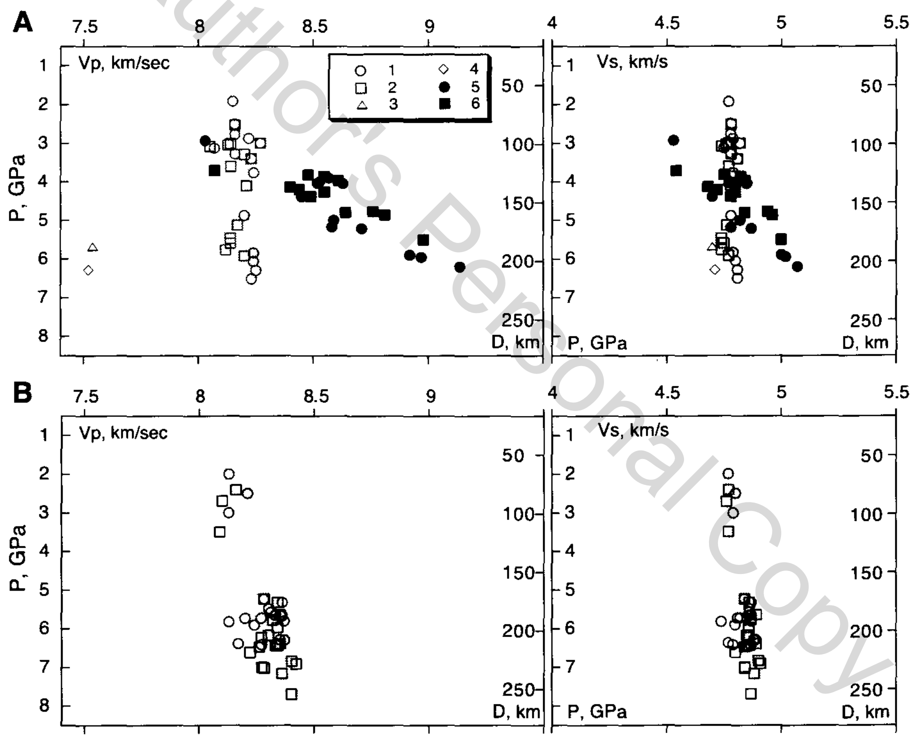

Fig. 3. Variation of seismic velocities with depth in the Jericho mantle (A) and the 5034 mantle (B). Symbols for seismic velocities estimated for individual xenoliths are: 1 and 2—peridotites at P–T conditions calculated according to the FB-MC method and the BKN-BK method; 3 and 4—pyroxenites at P–T conditions calculated according to the FB-MC method and the BKN-BK method; 5 and 6—eclogites estimated according to the Ai-FB method and the EG-BK method. Estimates for eclogites and pyroxenites are not available for the 5034 kimberlite. Grey fields are V–depth profiles computed for average pyroxenite and average peridotites by type at P–T conditions estimated according to the FB-MC method and the BK-BKN method (Table 3). There is a good agreement between seismic velocity estimates for individual and averaged peridotites, but the pyroxenite sample is not representative of a larger group of averaged pyroxenites.

(< 1 rel.%) and 0.15 km/s (< 3 rel.%) between the Reuss velocities and the Hill velocities for peridotite and eclogite (Supplementary Electronic Table 4).

Fig. 3 also illustrates seismic wave velocities in various peridotite types with averaged mineralogy. These velocities are computed for lower and upper limits of pressure and temperature determined for the rock types of Table 3, e.g. for spinel peridotite immediately below the Moho, and to $P = 33$ kb, respectively.

The profiles show that Vp in the Jericho peridotite increases slightly from 8.2 km/s below the crust to 8.3 km/s at 210 km. A similar gentle increase with depth from 8.1–8.2 km/s below the Moho to 8.45 km/s at 260-km depth is observed for the 5034 peridotites. The shear wave velocity in peridotite increases with depth even less, from 4.8 to 4.85 km/s. Because recalculation of surface seismic wave velocities to ambient $P-T$ conditions at depth decreases them (Table 3), commonly observed increasing velocity profiles in the upper mantle (Kennett and Engdahl, 1991) must be controlled by consistent changes in the mantle mineralogy with depth. Pyroxenites have significantly lower Vp's (7.5–7.6 km/s) and Vs's similar to those of peridotite. The seismic velocity profiles for eclogite feature a steep increase with depth, from 8.0 km/s at 100 km to 9.2 km/s at 200 km, "cutting through" the peridotite profile. The Vs profile for eclogite also cross-cuts the analogous peridotite profile.

The contrasting velocity–depth gradients of peridotite and eclogite are expected based on experimental pressure and temperature derivatives of their elastic constants (Table 4). In peridotite, an increase in seismic wave velocities due to higher pressure ($\Delta Vp^P \sim 0.35$ km/s) is offset by a decrease due to higher temperature ($\Delta Vp^T \sim -0.38$ km/s). This leads to practically constant modelled velocities independent of depth, or to a slight decrease in Vp with depth along higher geotherms (Jackson et al., 1990, O'Reilly et al., 1990; Weiss et al., 1999). In eclogite, seismic waves propagate more quickly with increasing pressure ($\Delta Vp^P = 0.5$ km/s) but the temperature effect is less pronounced ($\Delta Vp^T = -0.2$ km/s). The disparity in the derivatives for eclogite and peridotite arises from contrasting first-order pressure derivatives of bulk isotropic moduli. They are much lower in peridotite than in eclogite (Table 5) because the olivine modulus increases with pressure at a lower rate than that of pyroxenes and garnet (compare their Ks′ in Table 1 of Hofmeister and Mao, 2003). Another effect that contributes to the contrasting behavior of eclogite and peridotite at depth is the lower compressibility of eclogite at high pressures. Lower Andersen–Gruneisen parameters for eclogite reflect its smaller increase in density at depth ($\Delta\rho \sim 0.008$ in eclogite vs. 0.012 g/cm^3 in peridotite, Table 5).

The modelled profiles represent the expected wave velocities in mantle lithologies at depth at times preceding kimberlite eruption, i.e. in the Jurassic for Jericho and in the Cambrian for the 5034. As such, they reflect Jurassic and Cambrian steady-state geotherms. However, the deeper part (>160 km) of the Jericho profiles may not be representative of the steady-state mantle. Temperatures in this part of the mantle were reported to be 100–200 °C higher due to transient thermal perturbations and interactions with asthenospheric fluids (Kopylova et al., 1999a). Thus, at Jericho, the modelled velocities at depths greater than 160–190 km may be slightly lower than those typical of the ambient mantle, recording the unusual state of the upper mantle that precedes generation of kimberlitic magma.

7. Discussion

7.1. Model profiles in comparison with seismic surveys of the Slave craton

The predominantly peridotitic mantle of the Slave craton is modelled to have Vp increasing from 8.2 to 8.4 km/s and Vs from 4.8 to 4.9 km/s at depths of 35–260 km. These velocities can be compared to corresponding values derived from seismic studies of the Slave mantle. Two sets of data based on travel time Ps tomography are available for the Slave craton. Ramesh et al. (2002) report that the Canadian region has a normal upper mantle, in accordance with the *IASP91* model of Kennett and Engdahl (1991), and is underlain by a uniform normal mantle transition zone. The study of Bank et al. (2000) found that the Slave mantle is slightly faster than the global average of the *IASP91* model. An analysis of receiver functions with respect to the peak defining the discontinuity at 410 km can estimate the magnitude of the higher velocities postulated for the Slave mantle. Assuming that the shift of the peak to earlier times relative to *IASP91* was produced in the upper 410 km of the mantle, S-wave velocities should be higher by 0.05 km/s (Bostock, personal communication). These are the only velocity estimates available for the Slavic mantle. Here, the quilt-like structure of the mantle consists of laterally and vertically distinct domains (Grütter et al., 1999; Jones et al., 2001). This prevents any extrapolations of absolute seismic velocites estimated for the SW Slave in refraction studies (Fernandez Viejo and Clowes, 2003) to other parts of the Slave craton.

The range of seismic velocities permitted by mineralogy of Slave mantle rocks would expand if anisotropy is accounted for. It is generally thought to relate to lattice preferred orientations (LPO) of olivine and pyroxenes which can be measured microstructurally and experimentally (i.e. Soedjatmiko and Christensen, 2000; Ben-Ismail et al., 2001). The contribution of LPO to anisotropy of cratonic peridotite was calculated to be in the range of 2–8% for P-waves and 1–6% for S-waves for ~ 50 Kaapvaal xenoliths irrespective of their coarse or sheared textures (Ben-Ismail et al., 2001). A combined study of laboratory measurements and numerical calculations on a smaller set of cratonic xenoliths yielded similar values, 4.4–5.4% for Vp and 3.4–4.4% for Vs (Long and Christensen, 2000). In the absence of our own LPO data for Slave peridotite samples, we accept these estimates as an approximation of their average anisotropy. The anisotropy differentially expands the permissible limits of seismic velocities in the Jericho peridotitic mantle to higher values (Fig. 4). The regular *IASP91* mantle, as suggested for the Slave craton by Ramesh et al. (2002), and a 0.05 km/s faster mantle (Bostock, personal communication) fit equally well within the range of modelled peridotitic Vp's.

7.2. Effect of chemical depletion on elastic properties

Our calculations permit a quantitative assessment of bulk compositional effects on seismic velocities of cratonic mantle. The first and foremost of them is the effect of chemical depletion. It is well known based on model calculations that fertile mantle is slower (Jordan, 1979). Seismic velocities in the primitive mantle are up to 0.07 km/s slower than those in the more depleted subcontinental lithosphere (8.07 vs. 8.00 km/s for Vp and 4.68 vs. 4.65 km/s for Vs at 30 km; Weiss et al., 1999). Our data suggest that this

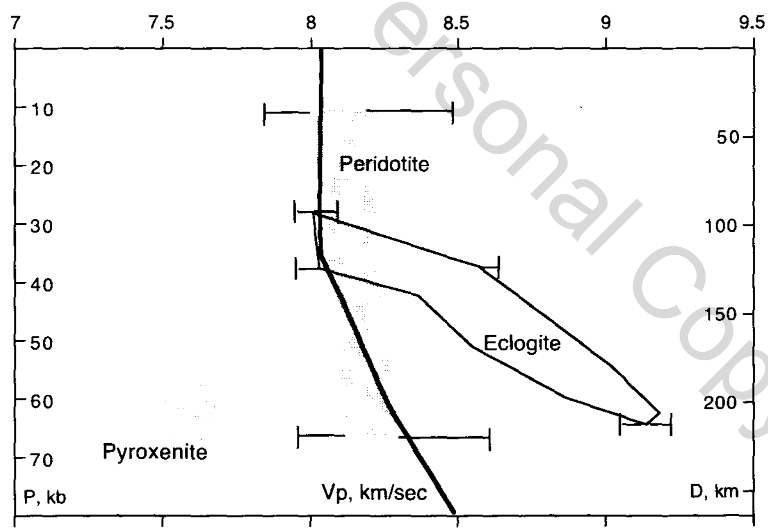

Fig. 4. Calculated Vp–depth profiles for Jericho mantle lithologies in comparison with a globally averaged *IASP91* model (Kennett and Engdahl, 1991) profile (bold). Ranges of velocities in isotropic peridotite and pyroxenite (grey) and eclogite (open field) are from Fig. 3. Bars designate the extent of seismic anisotropy expected in these rocks and equal 2% in eclogite (based on experimental values for homogeneous and unaltered samples) and 5% in peridotite. The bars are asymmetric (2 times closes to the minimum than maximum anisotropic Vp) about the range of isotropic velocity in peridotite.

pattern is true only of circumcratonic and oceanic mantle, i.e. of the mantle stabilized in the Phanerozoic and found as abyssal peridotites, peridotite massifs and mantle xenoliths in Phanerozoic settings. The composition of cratonic peridotite is anomalous in many aspects. Cratonic harzburgites and lherzolites show inverse correlations of olivine mode with depletion expressed as Mg-number, whereas olivine mode increases with the peridotite Mg-number in off-craton samples (Fig. 9 in Griffin et al., 1999a,b). Many xenoliths from Archean cratons are characterized by extreme depletion, abundant orthopyroxene, and low olivine/orthopyroxene ratios (Boyd, 1989; Kelemen et al., 1998; Griffin et al., 1999a,b).

In the Slave mantle, P-waves travel slower and S-waves faster in more depleted peridotites, thus defining a visible decrease in the Poisson's ratio (Fig. 5B–D). We ascribe this to a correlation between depletion and orthopyroxene modes (Fig. 5A). This correlation is apparent in data averaged by peridotite types, but is masked by sample heterogeneity if sought in individual specimens of peridotite.

Peridotites below other cratons do not show the visible correlation between orthopyroxene modes and rock Mg-numbers, but an intrinsic link between the two is suggested by common orthopyroxene enrichment in high Mg-number peridotites (Kelemen et al., 1998). The correlation may be implied by several other chemical characteristics of cratonic peridotites, i.e. a negative correlation between Mg-number and olivine mode (Griffin et al., 1999a,b), and between bulk SiO_2 and FeO (Boyd, 1989, 1999; Kopylova and Russell, 2000). Since orthopyroxene is the second

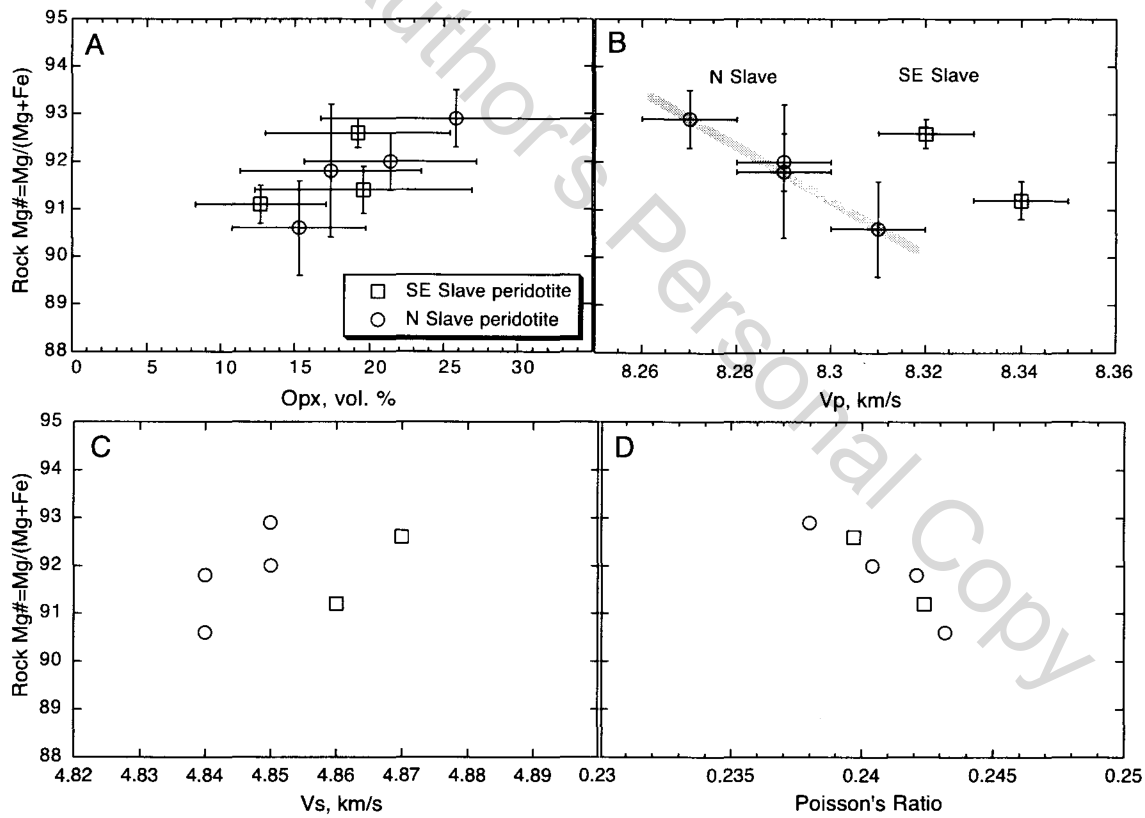

Fig. 5. Variation of geochemical and elastic parameters of the Slave peridotitic mantle with depletion, expressed as rock Mg-number. The data are averaged by rock type and can be found in Table 3 of this work and Table 3 of Kopylova and Caro (2004). Error bars plotted for Opx modes and Mg-numbers represent 2σ standard deviations of the data sets. Mg-numbers are plotted against orthopyroxene mode (A), Vp (B), Vs (C), and Poisson's ratio (D). The latter is defined as $\sigma=(3K_S-2G)/(6K_S+2G)$.

major phase of cratonic peridotite, and modes of clinopyroxene and garnet rarely exceed 5%, the cratonic olivine-poor peridotites with high Mg-numbers should be richer in orthopyroxene. Because bulk FeO and MgO are inversely related, and SiO_2 is controlled mainly by the orthopyroxene/olivine ratio, there should be a correlation between Mg-number of cratonic peridotite and its orthopyroxene mode. These predicted correlations can be hard to isolate if mineral modes and mineral compositions are recalculated based on bulk chemical compositions of peridotites (e.g. Kelemen et al., 1998), which are rarely fresh. Thorough petrographic studies of cratonic peridotite and direct measurements of mineral modes and compositions in thin sections are needed to map the orthopyroxene–Mg# correlation.

The above data can be summarized to suggest a distinct seismic signature for depletion in cratonic mantle. The depleted mantle below cratons should be slower in Vp, faster in Vs and should show lower Poisson's ratios than the less depleted mantle. The calculated effect should depend on the overall compositional range of peridotite and may differ from craton to craton. On the Slave craton, the restricted range of depleted bulk compositions suggests the effect on Vp or Vs would be up to 0.05 km/s.

Our modelling of seismic velocities forecasts different responses of Vp and Vs to depletion of cratonic mantle. Similar conclusion was reached in a recent study on modelled elastic properties of mantle peridotite (Lee, 2003). Lee found that the trend of correlated increase of Vs with increasing Mg-number is tight and well defined ($R^2 = 0.71$). In contrast, the covariation of Vp and Mg-number cannot be characterised by an apparent trend for the entire data set. A positive correlation of Vp and Mg-number is evident only for spinel peridotite that plot on a melt depletion trend ("oceanic array" of Boyd, 1989). Garnet peridotites, many of which are from cratonic localities and plot off the melt depletion trend, form a large scattered field on the Vp-Mg-number diagram with barely recognizable negative correlation (Fig. 11 in Lee, 2003).

The only reason model seismic wave velocities increase over the range of 30–250-km depth in the Slave peridotite is the consistently lower degree of chemical depletion in the deeper mantle. A mantle with a uniform composition would show decreasing Vp and Vs with depth according to our models. A consistent decrease in degree of depletion with depth is recorded in garnet concentrate data (Gaul et al., 2000; Griffin et al., 2003) for many Archean, Proterozoic and some Phanerozoic subcontinental mantle columns. Commonly observed increasing Vp, Vs depth profiles in the mantle as tabulated in *IASP91* suggest that the progressively lower depletion of the peridotite with depth should be a widespread phenomenon.

Another important elastic parameter of the mantle is density. Calculated densities of various peridotite types increase consistently from shallow spinel peridotite to deep garnet-bearing peridotite types (Table 4). Density increases from 3.286–3.287 g/cm^3 in depleted spinel peridotite to 3.319 and 3.340 g/cm^3 in the high-T and fertile peridotites. This density profile is gravitationally stable and is consistent with the long-stabilized mantle system. Densities of 3.28 g/cm^3 in the Slave depleted spinel peridotite are lower than the average (3.31 ± 0.016 g/cm^3, Poudjom Djomani et al., 2001) for the Archean cratonic mantle.

7.3. Effect of metasomatism on elastic properties of eclogite

Mantle metasomatism partially melts Jericho eclogite and leads to partial replacement of the primary omphacite–garnet assemblage. The secondary assemblage thus produced comprises fine-grained diopside, pyrope, phlogopite and amphibole. We calculated model seismic velocities for the metasomatized eclogite (Table 3) and found them to be invariably lower than those in eclogite not affected by metasomatism. Recrystallization of 14% primary clinopyroxene and 31% garnet into corresponding secondary phases lowers Vp from 8.13 to 8.09 km/s and leaves Vs unchanged (Sample 52-5). Introduction of 6% amphibole and recrystallization of 36% clinopyroxene, as in sample 47-8, lowers Vp more substantially, from 8.00 to 7.82 km/s, and Vs from 4.61 to 4.52 km/s. We conclude that metasomatic recrystallization of eclogite in the Slave mantle decreases P-wave velocities in the order of 0.05–0.1 km/s.

8. Conclusions

1. Seismic profiles calculated for the Slave mantle peridotites based on their mineralogy match well

with the globally averaged *IASP91* model. The calculated spread of Vp related to variations in mantle mineralogy at a given depth reaches 0.3 km/s in peridotite and 0.4 km/s in eclogite.

2. Seismic velocities in eclogite increase faster with depth than those in peridotite. A faster mantle below 90-km depth on the Slave craton can be explained by an unusually high proportion of eclogite.
3. Depletion in the cratonic mantle has a distinct seismic signature compared to the non-cratonic mantle stabilized in the Phanerozoic. The depleted mantle on cratons should have slower Vp, faster Vs and should show lower Poisson's ratios due to an orthopyroxene enrichment. On the Slave craton, the predicted effect on seismic wave velocities would be up to 0.05 km/s.
4. The consistently lower degree of chemical depletion in the deeper Slave mantle is the sole reason for the increase in the modelled seismic wave velocities at 30–250—km depth.

Acknowledgements

Funding for this research is derived from the Natural Sciences and Engineering Research Council (NSERC) of Canada. We are grateful to M Bostock and C. Bank for useful discussions on the topic of the manuscript, and to D. Mainprice, A. Jones and H. Grütter for reviews and editorial suggestions.

References

Ai, Y., 1994. A revision of the garnet-clinopyroxene Fe^{2+}–Mg exchange geothermometer. Contrib. Mineral. Petrol. 115, 467–473.

Angel, R.J., Hugh-Jones, D.A., 1994. Equations of state and thermodynamic properties of enstatite pyroxenes. J. Geophys. Res. 99, 19777–19783.

Bank, C.G., Bostock, M.G., Ellis, R.M., Cassidy, J.F., 2000. A reconnaissance teleseismic study of the upper mantle and transition zone beneath the Archean Slave craton in NW Canada. Tectonophysics 319, 151–166.

Bass, J.D., 1986. Elasticity of uvarovite and andradite garnets. J. Geophys. Res 91, 7505–7515.

Ben-Ismail, G., Barruol, D., Mainprice, A., 2001. The Kaapvaal seismic anisotropy: petrophysical analyses of upper mantle kimberlite nodules. Geophys. Res. Lett. 28 (13), 2497–2500.

Bina, C.R., Helffrich, G.R., 1992. Calculations of elastic properties from thermodynamic equation of state principles. Annu. Rev. Earth Planet Sci. 20, 527–552.

Boyd, F.R., 1989. Compositional distinction between oceanic and cratonic lithosphere. Earth Planet. Sci. Lett. 96, 15–26.

Boyd, F.R., 1999. The origin of cratonic peridotites: a major-element approach. In: Snyder, G.A., Neal, C.R., Ernst, W.G. (Eds.), Planetary Petrology and Geochemistry; the Lawrence A. Taylor 60th Birthday Volume. Bellwether Publishing, Columbia, pp. 5–14.

Brey, G.P., Köhler, T., 1990. Geothermobarometry in four-phase iherzolites: II. New thermobarometers, and practical assessment of existing thermobarometers. J. Petrol. 31, 1353–1378.

Chai, M., Brown, M., Slutsky, L.J., 1997. The elastic constants of an aluminous orthopyroxene to 12.5 GPa. J. Geophys. Res. 102, 14779–14785.

Chang, Z.P., Barsch, G.R., 1973. Pressure dependence of single-crystal elastic constants and anharmonic properties of spinel. J. Geophys. Res. 78, 2418–2433.

Chen, G.L., Spetzler, H.A., Getting, I.C., Yoneda, A., 1996. Selected elastic moduli and their temperature derivatives for olivine and garnet with different Mg/(Mg + Fe) contents: results from GHz ultrasonic interferometry. Geophys. Res. Lett. 23, 5–8.

Christensen, N.I., 1965. Compressional wave velocities in metamorphic rocks at pressures to 10 kb. J. Geophys. Res. 70, 6147–6164.

Christensen, N.I., 1989. Seismic velocities. In: Carmichael, R.S. (Ed.), CRC Handbook of Physical Properties of Rocks. CRC Press, Boca Raton, Florida, pp. 206–531.

Christensen, N.I., Shaw, G.H., 1970. Elastisity of mafic rocks from the mid-Atlantic ridge. Geophys. J. R. Astron. Soc. 20, 271–284.

Collins, M.D., Catlow, C.R.A., 1992. Computer simulation of structures and cohesive properties of micas. Am. Mineral. 77, 1172–1181.

Duffy, T.S., Ahrens, T.J., 1995. Compressional sound velocity, equation of state and constitutive response of shock-compressed magnesium oxide. J. Geophys. Res. 100, 529–542.

Duffy, T.S., Anderson, D.L., 1989. Seismic velocities in mantle minerals and the mineralogy of the upper mantle. J. Geophys. Res. 94, 1895–1912.

Ellis, D.J., Green, D.H., 1970. An experimental study of the effect of Ca upon garnet–clinopyroxene Fe–Mg exchange equilibria. Contrib. Mineral. Petrol. 71 (1), 13–22.

Fei, Y., 1995. Thermal expansion. In: Ahrens, T.J. (Ed.), Mineral Physics and Crystallography: A Handbook of Physical Constants. AGU, Washington, pp. 29–44.

Fernandez Viejo, G., Clowes, R.M., 2003. Lithospheric structure beneath the Archean Slave Province and Proterozoic Wopmay orogen, northwestern Canada, from a LITHOPROBE refraction/wide-angle reflection study. Geophys. J. Int. 153, 1–19.

Finnerty, A.A., Boyd, J.J., 1987. Thermobarometry for garnet peridotites: basis for the determination of thermal and compositional structure of the upper mantle. In: Nixon, P.H. (Ed.), Mantle Xenoliths. Wiley, New York, pp. 381–402.

Flesch, L.M., Li, B., Liebermann, R.C., 1998. Sound velocities of polycrystalline $MgSiO_3$- orthopyroxene to 10 GPa at room temperatures. Am. Mineral. 83, 444–450.

Gaul, O.F., Griffin, W.L., O'Reilly, S.Y., Pearson, N.J., 2000. Mapping olivine composition in the lithospheric mantle. Earth Planet. Sci. Lett. 182, 223–235.

Gregoire, M., Jackson, I., O'Reilly, S.Y., Cottin, J.Y., 2001. The lithospheric mantle beneath the Kerguelen Islands (Indian Ocean): petrological and petrophysical characteristics of mantle mafic rock types and correlation with seismic profiles. Contrib. Mineral. Petrol. 142, 244–259.

Griffin, W.L., O'Reilly, S.Y., Ryan, C.G., 1999a. The composition and origin of sub-continental lithospheric mantle. In: Fei, Y., Bertka, C.M., Mysen, B.O. (Eds.), Mantle Petology: Field Observations and High-Pressure Experimentation: A Tribute to F.R. Boyd. The Geochemical Society Special Publication, No., 6. The Geochemical Society, Houston, pp. 13–45.

Griffin, W.L., Doyle, B.J., Ryan, C.G., Pearson, N.J., O'Reilly, S.Y., Natapov, L., Kivi, K., Kretschmar, U., Ward, J., 1999b. Lithosphere structure and mantle terranes: Slave craton, Canada. In: Gurney, J.J., Gurney, J.L., Pascoe, M., Richardson, S.R. (Eds.), Proc. 7th Int. Kimberlite Conference. Red Roof Designs, Cape Town, pp. 299–306.

Griffin, W.L., O'Reilly, S.Y., Doyle, B.J., Kivi, K., Coopersmith, H.G., 2003. Lithospheric mapping benarth the North American plate. Extended Abstract, 8th Intern Kimb Conf., June 2003, Victoria, Canada.

Grütter, H.S., Apter, D.B., Kong, J., 1999. Crust–mantle coupling: evidence from mantle-derived xenocrystic garnets. In: Gurney, J.J., Gurney, J.L., Pascoe, M., Richardson, S.R. (Eds.), Proc. 7th Int. Kimberlite Conference. Red Roof Designs, Cape Town, pp. 307–312.

Heaman, L.M., Kjarsgaard, B., Creaser, R.A., 2003. The timing of kimberlite magmatism and implications for diamond exploration; a global perspective. Lithos 71, 153–184.

Hearmon, R.F.S., 1984. The elastic constants of crystals and other anisotropic materials. In: Hellwage, K.H., Hellwage, A.M. (Eds.), Landolt-Bornstein Tables, III/18. Springer, Berlin, pp. 1–54.

Hofmeister, A.M., Mao, H.K., 2003. Pressure derivatives of shear and bulk moduli from the thermal Gruneisen parameter and volume–pressure data. Geochim. Cosmochim. Acta 67 (7), 1207–1227.

Isaak, D.G., Anderson, O.L., Oda, H., 1992. High-temperature thermal-expansion and elasticity of calcium-rich garnets. Phys. Chem. Miner. 19, 106–120.

Isaak, D.G., Carnes, J.D., Anderson, O.L., Cynn, H., Hake, E., 1998. Elastisity of TiO2 rutile to 1800 K. Phys. Chem. Miner. 26, 31–43.

Jackson, I., Rudnick, R.L., O'Reilly, S.Y., Bezant, C., 1990. Measured and calculated elastic wave velocities for xenoliths from the lower crust and upper mantle. Tectonophysics 173, 207–210.

Ji, S., Wang, Q., Xia, B., 2003. P-wave velocities of polymineralic rocks: comparison of theory and experiment and test of elastic mixture rules. Tectonophysics 166, 165–185.

Jones, A., Ferguson, I., Chave, A., Evans, R., McNeice, G., 2001. Electric lithosphere of the Slave craton. Geology 29, 423–426.

Jordan, T.H., 1979. Mineralogies, densities and seismic velocities of garnet lherzolites and their geophysical implications. In: Boyd, F.R., Meyer, H.O.A. (Eds.), The Mantle Sample: Inclusions in Kimberlites and Other Volcanics. AGU, Washington, pp. 1–15.

Kandelin, J., Weidner, D.J., 1998. The single crystal elastic properties of jadeite. Phys. Earth Planet. Inter. 50, 251–260.

Kelemen, P.B., Hart, S.R., Bernstein, S., 1998. Silica enrichment in the continental upper mantle via melt/rock reaction. Earth Planet. Sci. Lett. 164, 387–406.

Kennett, B.L.N., Engdahl, E.R., 1991. Travel times for global earthquake location and phase identification. Geophys. J. Int. 105, 429–465.

Kern, H., Gao, S., Jin, Z., Popp, T., Jin, S., 1999. Petrophysical studies of rocks from the Dabie ultrahigh-pressure (UHP) metamorphic belt, Central China: implications for the composition and delamination of the lower crust. Tectonophysics 301, 191–215.

Ketchum, J.W.F., Bleeker, W., 2001. 4.03–2.85 Ga growth and modification of the Slave protocraton, NW Canada. Abstract, The Slave–Kaapvaal Workshop, Sept. 2001, Merrickville.

Kopylova, M.G., 2003. Two distinct origins of the Northern Slave eclogites. Ext. Abstract of the 8th Intern. Kimb. Conf., Victoria, June.

Kopylova, M.G., Caro, G., 2004. Mantle xenoliths from the Southeastern Slave craton: The evidence for a thick cold stratified lithosphere. J Petrol. 45 (5), 1045–1067.

Kopylova, M.G., Russell, J.K., 2000. Chemical stratification of cratonic lithosphere: constraints from the Northern Slave Craton, Canada. Earth Planet. Sci. Lett. 181, 71–87.

Kopylova, M.G., Russell, J.K., Cookenboo, H., 1999a. Petrology of peridotite and pyroxenite xenoliths from the Jericho kimberlite: implications for the thermal state of the mantle beneath the Slave Craton, Northern Canada. J. Petrol. 40 (1), 79–104.

Kopylova, M.G., Russell, J.K., Cookenboo, H., 1999b. Mapping the lithosphere beneath the North Central Slave Craton. In: Gurney, J.J., Gurney, J.L., Pascoe, M.D., Richardson, S.H. (Eds.), Proceedings of the VIIth International Kimberlite Conference, vol. 1 Red Roof Design, Cape Town, pp. 468–479.

Lee, C.A., 2003. Compositional variation of density and seismic velocities in natural peridotites at STP conditions: implications for seismic imaging of compositional heterogeneities in the upper mantle. J. Geophys. Res. 108 (B9), 2441–2462.

Li, B., Gwanmesia, G.D., Liebermann, R.C., 1996. Sound velocities of olivine and beta polymorphs of Mg_2SiO_4 at Earth's transition zone pressures. Geophys. Res. Lett. 23, 2259–2262.

Long, C., Christensen, N.I., 2000. Seismic anisotropy of South African upper mantle xenoliths. Earth Planet. Sci. Lett. 179, 551–565.

MacGregor, I.D., 1974. The System MgO–Al_2O_3–SiO_2: solubility of Al_2O_3 in enstatite for spinel and garnet peridotite compositions. Am. Mineral. 59, 110–119.

McCammon, C., Kopylova, M.G., accepted pending revisions. A redox profile of the Slave mantle and oxygen fugacity control in the cratonic mantle. Contrib. Miner. Petrol.

O'Neill, H.S.C., Wood, B.J., 1979. An experimental study of Fe–Mg partitioning between garnet and olivine and its calibration as a geothermometer. Contrib. Mineral. Petrol. 70, 59–70 (corrected in Contrib Mineral Petrol, 1980, 72, 337).

O'Reilly, S.Y., Jackson, I., Bezant, C., 1990. Equilibration temperatures and elastic wave velocities for upper mantle rocks from Eastern Australia: implications for the interpretation of seismological models. Tectonophysics 185, 67–82.

Poudjom Djomani, Y.H., O'Reilly, S.Y., Griffin, W.L., Morgan, P., 2001. The density structure of subcontinental lithospher through time. Earth Planet. Sci. Lett. 184, 605–621.

Ramesh, D.S., Kind, R., Yuan, X., 2002. Receiver function analysis of the North American crust and upper mantle. Geophys. J. Int. 150, 91–108.

Soedjatmiko, B., Christensen, N.I., 2000. Seismic anisotropy under estended crust: evidence from upper mantle xenoliths, Cima Volcanic Field, California. Tectonophysics 321, 279–296.

Sumino, Y., Anderson, O.L., 1984. Elastic constants of minerals. In: Carmichael, R.S. (Ed.), Handbook of Physical Properties of Rocks. CRC Press, Boca Raton, pp. 39–137.

Thorpe, R.I., Cumming, G.L., Mortensen, J.K., 1992. A major Pb-isotope boundary in the Slave Province and its probable relation to ancient basement of the western Slave. Canada-NWT MDA summary volume. Geol. Surv. Can., Open File 2484, 179–184.

Vacher, P.A., Mocquet, A., Sotin, C., 1998. Computation of seismic profiles from mineral physics: the importance of the non-olivine components for explaining the 660 km depth discontinuity. Phys. Earth Planet. Inter. 106, 275–298.

Wang, H., Simmons, G., 1972. Elastisity of some mantle crystal structures: 1. Pleonaste and hercynite spinel. J. Geophys. Res. 77, 4379–4392.

Weidner, D.J., Ito, E., 1985. Elasticity of $MgSiO_3$ in the ilmenite phase. Phys. Earth Planet. Inter. 40, 65–70.

Weiss, T., Siegesmund, S., Bohlen, T., 1999. Seismic, structural and petrological models of the subcrustal lithosphere in Southern Germany: a quantitative re-evaluation. Pure Appl. Geophys. 156, 53–81.

Welch, M.D., Crichton, W.A., 2002. Compressibility of clinochlore to 8 GPa at 298 K and a comparison with micas. Eur. J. Mineral. 14, 561–565.

Yang, H.M., Prewitt, C.T., 2000. Chain and layer silicates at high temperatures and pressures. In: Hazen, R.M., Downs, R.T. (Eds.), High-Temperatures and High-Pressure Crystal ChemistryReviews in Mineralogy and Geochemistry, vol. 41. Mineralogical Society of America and Geochemical Society of America, Washington, pp. 211–255.

Yoneda, A., 1990. Pressure derivatives of elastic constants of single crystal MgO and $MgAl_2O_4$. J. Phys. Earth 38, 19–55.

Zha, C.S., Duffy, T.S., Downs, R.T., Mao, H.K., Hemley, R.J., 1996. Sound velocity and elasticity of single-crystal forsterite to 16 GPa. J. Geophys. Res. 101 (B8), 17535–17545.

Zha, C.S., Duffy, T.S., Mao, H.K., Downs, R.T., Hemley, R.J., Weidner, D.J., 1997. Single-crystal elasticity of beta-Mg_2SiO_4 to the pressure of the 410 km seismic discontinuity in the Earth's mantle. Earth Planet. Sci. Lett. 147, 9–15.

Zhang, L., Ahsbahs, H., Hafner, S.S., Kutoglu, A., 1997. Single-crystal compression and crystal structure of clinopyroxene up to 10 GPa. Am. Mineral. 82, 245–258.

Zhao, Y.S., VonDreele, R.B., Shankland, T.J., Weidner, D.J., Zhang, J.Z., Wang, Y.B., Gasparik, T., 1997. Thermoelastic equation of state of jadeite $NaAlSi_2O_6$: an energy-dispersive reitveld refinement study of low symmetry and multiple phases diffraction. Geophys. Res. Lett. 24, 5–8.